

1 Title: Exploring the Lightning Jump Characteristics

2 Authors:

3 T. Chronis¹, L. D. Carey¹, C. J. Schultz^{1,2}, E. V. Schultz¹, K. M. Calhoun³, and S. J.
4 Goodman⁴

5 ¹ University of Alabama in Huntsville, Earth System Science Center

6 ² NASA Marshall Space Flight Center

7 ³ Oklahoma University Cooperative Institute of Mesoscale Meteorology Studies,
8 National Severe Storm Laboratory,

9 ⁴ NOAA Satellite and Information Service (NESDIS)

10

11 Corresponding Author: Themis Chronis, themis.chronis@nsstc.uah.edu

12 University of Alabama in Huntsville

13 Earth System Science Center

14 320 Sparkman Dr., Huntsville 35805, AL

15

16

17

18

19

20

21

22 **Abstract**

23 This study is concerned with the characteristics of storms exhibiting an abrupt temporal
24 increase in the total lightning flash rate (i.e., lightning jump, LJ). An automated storm
25 tracking method is used to identify storm “clusters” and total lightning activity from
26 three different lightning detection systems over Oklahoma, northern Alabama and
27 Washington, D.C. On average and for different employed thresholds, the clusters that
28 encompass at least one LJ (LJ1) last longer, relate to higher Maximum Expected Size of
29 Hail, Vertical Integrated Liquid and lightning flash rates (area-normalized) than the
30 clusters that did not exhibit any LJ (LJ0). The respective mean values for LJ1 (LJ0)
31 clusters are 80 min (35 min), 14 mm (8 mm), 25 kg m⁻² (18 kg m⁻²) and 0.05 flash min⁻¹
32 km⁻² (0.01 flash min⁻¹ km⁻²). Furthermore, the LJ1 clusters are also characterized by
33 slower decaying autocorrelation functions, a result that implies a less "random" behavior
34 in the temporal flash rate evolution. In addition, the temporal occurrence of the last LJ
35 provides an estimate of the time remaining to the storm’s dissipation. Depending of the
36 LJ strength (i.e., varying thresholds), these values typically range between 20-60 min,
37 with stronger jumps indicating more time until storm decay. This study’s results support
38 the hypothesis that the LJ is a proxy for the storm’s kinematic and microphysical state
39 rather than a coincidental value.

40 **1. Introduction**

41 The advent of ground-based lightning detection networks in recent decades has
42 made real-time retrieval of total lightning activity (cloud-to-ground, CG and the intra-

43 cloud, IC) available in both high spatial and temporal resolutions. Although there are
44 uncertainties in the details (Takahashi 1978; Saunders 1993), it is known that
45 rebounding collisions between graupel and ice crystals in the presence of super-cooled
46 water is the primary process for thunderstorm electrification (MacGorman and
47 Morgenstern 1998; Saunders et al. 2006; Emersic and Saunders 2010). Several studies
48 have documented a temporal co-variability between updraft mass flux, precipitation ice
49 mass and overall storm depth with the respective total lightning activity (e.g., Goodman
50 et al. 1988; Carey and Rutledge 2000; Chronis et al. 2007; Deierling and Petersen 2008;
51 Bruning and MacGorman 2013). Hence, it would be reasonable to suggest that an abrupt
52 temporal change of the order of a few minutes in the total lightning activity is
53 considered as a severe weather indicator ("Lightning Jump", LJ, see Schultz et al. 2009;
54 2011). Studies by Williams et al. (1999), Gatlin and Goodman (2010), Carey et al.
55 (2009), Schultz et. al. (2009; 2011) and Rudlosky and Fuelberg (2013) document that
56 statistics such as lead time, probability of detection and false alarm ratio could be
57 improved based on the use of total lightning as a metric for storm intensity. Nonetheless,
58 these methods can be hindered by problems related to uncertainties in severe weather
59 observations at the surface (Trapp et al. 2006; Keene et al. 2008; Schultz et al. 2011).
60 This study puts forward an original comparison between the convective characteristics
61 of storms that did or did not exhibit a LJ throughout their lifetime. This evaluation relies
62 on radar-derived and lightning properties.

63 **2. Data and Methods**

2.1 Storm Tracking and Clustering

The storm identification and tracking have been performed in real-time utilizing the Warning Decision Support System Integrated Information tracking system (WDSS-II, Lakshmanan et al. 2007). A storm “cluster” is automatically identified by the reflectivity across the -10°C isothermal layer, following a merger of individual WSR-88D radars. A combination of watershed segmentation and k-means clustering is employed to identify the storm clusters (Lakshmanan et al. 2009; Kolodziej Hobson et al. 2012; Cintineo et al. 2014). To complete the storm identification, the algorithm searches for local reflectivity (Z) maxima where $Z > 20$ dBZ, then incrementally grows the area until it is at least 200 km^2 . The storm cluster is then matched with a separately identified cluster at the next time step (for our analysis, a 1-min time step was used) using a cost function, where longer-lived cells are given preference in the case of storm mergers.

Each storm (hereinafter cluster) is described by a geolocated polygon (i.e. footprint). The cluster’s lifespan is determined as the total time a cluster was identified and tracked by WDSS-II (Lakshmanan and Smith 2009). The Maximum Vertical Integrated Liquid (VIL, Greene and Clark 1972) and the Maximum Expected Size of Hail (MESH, Witt et al. 1998; Cintineo et al. 2012) are retrieved for each cluster for the duration of its lifetime. Both VIL and MESH have been used as radar-derived intensity metrics for storm properties such as liquid precipitation, updraft strength and hail growth (Amburn and Wolf 1996; Witt et al. 1998). As with any proxy, there are caveats that

85 reflect the imperfect representations of severe weather potential and emanate from
86 parameters unrelated to the storm dynamics (e.g. distance from the radar, tilted updrafts,
87 storm speed etc., Stumpf et al. 2004). To mitigate these effects as much as possible, all
88 available radars in the area are used to retrieve these proxies. Five radars over each of
89 the three locations are employed, namely, KFDR, KTLX, KVNK, KINX, KSRX for
90 Oklahoma, KHTX, KGWX, KBMX, KDHX, KFFC for north Alabama and KLWX,
91 KDOX, KAKQ, KCCX, KDIX for DC (radar acronyms from
92 <https://www.ncdc.noaa.gov/nexradinv/map.jsp>). The data for the present study extends
93 from 1 April 2013 through 14 August 2013.

94 *2.2 Total Lightning Activity and the Lightning Jump Algorithm*

95 This study employs three total lightning detection networks: 1) the Lightning
96 Mapping Array (LMA) networks located in central/SW Oklahoma (MacGorman et al.
97 2008), North Alabama (Goodman et al. 2005), and Washington D.C (Krehbiel 2008) 2)
98 the Earth Networks Total Lightning Network (ENTLN, Liu and Heckman 2010) and 3)
99 the National Lightning Detection Network (NLDN, Cummins et al. 1995,2005,
100 Cummins and Murphy 2009).

101 The LMA networks detect the very high frequency (VHF) radiation emitted
102 during the elemental processes that compose a lightning discharge (e.g. the initial
103 breakdown, leader propagation and other K-processes, Uman 1987) with a location
104 accuracy measured in tens of meters and with a time resolution of 80-100 μ s (Thomas et
105 al. 2004). The LMA detects both IC and CG flashes although the distinction can be

106 dubious due to limitations in range. The location accuracy is also range-dependent,
107 however it is relatively constant between ~150 km radius from the respective center
108 (Thomas et al. 2004; Koshak et al. 2004). The following analysis relies on the total
109 lightning flashes occurring within ~120 km of the respective LMA center (Thomas et al.
110 2003). Lightning flashes are retrieved from the LMAs via grouping at least 10 detected
111 VHF radiation sources, using time and space constraints (3 km and 150 ms) between the
112 adjoining points (McCaul et al. 2008). Only flashes that begin within the storm cluster's
113 footprint are counted towards the total flash rate. No classification between CG and IC
114 flashes is performed using LMA data.

115 The ENTLN sensors operate over a wide frequency range, spanning from 1 Hz to
116 12 MHz. According to Liu and Heckman (2011), electric field waveforms are used in
117 locating as well as classifying the IC and CG flashes. Multiple strokes (or individual
118 cloud events) are clustered into a single flash if they are within 700 ms and 10 km of the
119 first detected stroke. A flash that contains at least one return stroke is classified as a CG
120 flash, otherwise it is classified as an IC flash.

121 Since the late 1980s, the National Lightning Detection Network (NLDN,
122 Cummins et al. 1995; 1998; 2006) has served as the source for many CG lightning-
123 related studies over the US. The network consists of 113 sensors that combine the
124 advantages of direction finding and time-of-arrival techniques. The NLDN CG detection
125 efficiency ranges between 90-95% over the mid latitude continental US, with a median
126 location error better than 500 m (Cummins and Murphy 2009; Rudlosky and Fuelberg

127 2010). Although the NLDN is designed to primarily detect CG flashes, it has been
128 recently reported that IC flashes are also detected depending on the restrictions applied
129 to the processed waveforms (peak-to-zero rise time, Murphy and Nag, 2014).

130 The present study employs the total flash activity (IC+CG) for all lightning
131 detection systems. Rudlosky and Fuelberg (2013) use a similar methodology for
132 compiling lightning and radar data. Both NLDN and ENTLN have national (US)
133 coverage. Nevertheless, for this analysis the respective total lightning activity is
134 computed only for the clusters that are identified over a radius around where the
135 optimum LMA operation is ensured. Further detailed comparison (e.g., relative location
136 accuracy and detection efficiency) between the lightning detection systems lies outside
137 the scope of this paper. However, their employment is considered as a preliminary
138 attempt to demonstrate results pertaining to the LJ properties from lightning detection
139 networks of different technical specifications (e.g., detection efficiency).

140 The 1-min flash rate is computed by adding all the flashes occurring within the
141 footprint of the identified cluster. The LJ is objectively identified by Schultz et al. (2009;
142 2011). This technique uses 14 min of the cluster's most recent flash rate history. Twelve
143 of the 14 minutes are considered to calculate the minimum jump threshold that must be
144 exceeded for a LJ to occur. The remaining two minutes are used to determine whether
145 the current rate of change in the total flash rate exceeds the LJ threshold. As outlined in
146 Schultz et al. (2009; 2011), the algorithm is a 5-step process. These steps are as follows:
147 1) The total flash rate ($f \text{ min}^{-1}$) from the 14 minute period is binned into two minute

148 segments and the total flash rate is averaged (Eqn. 1)

$$149 \quad FR_{avg}(t) = \frac{FR(t)+FR(t-1)}{2} \quad (1)$$

150 2) The rate of change of the total flash rate (DFRDT, $f \text{ min}^{-2}$) is calculated by subtracting

$$151 \quad \text{consecutive bins from each other (Eqn. 2) } \frac{d}{dt} FR_{avg}(t) = \frac{FR_{avg}(t)-FR_{avg}(t-1)}{2} = DFRDT$$

$$152 \quad (2)$$

153 This results in six DFRDT values ($f \text{ min}^{-2}$) 3) The five earliest DFRDT values in time

154 are used to calculate the standard deviation (σ) of the population 4) If $DFRDT > \alpha * \sigma$

155 and the flash rate is in greater than a given flash rate threshold (FRT) then a LJ has

156 occurred. Note that α represents a multiplicative factor (i.e. dimensionless) and has no

157 relation to the standard deviation (σ). In the original studies by Schultz et al. (2009;

158 2011) α and FRT were set to 2.0 and $10 f \text{ m}^{-1}$. Also note that α is dimensionless (i.e., f

159 $\text{min}^{-2} / f \text{ min}^{-2}$). Here we compute the LJ based on a variable α (0.5 - 4, step of 0.5) and

160 FRT (5-25 $f \text{ m}^{-1}$, step of 5 $f \text{ m}^{-1}$). The latter is employed in order to define the LJ relative

161 strength. For example, a weaker LJ1 would have $\alpha=1.0$ and $FRT=10 f \text{ m}^{-1}$ while a

162 stronger LJ1 would be considered as $\alpha=2.0$ and a $FRT=15 f \text{ m}^{-1}$ 5) This process is

163 repeated every two minutes as new total lightning flash rates are collected until the

164 storm dissipates.

165 We note that the above implemented time-window within which the LJ is

166 calculated is based on empirical observations of the growth and decay on the convective

167 time scale (<10-20 minutes). Had we allowed for longer periods (e.g. 40-60 minutes)

168 into the thunderstorm's lifetime we would likely have missed the occurrence of the first
169 LJ and potentially severe weather occurrence. This is why we've empirically tested this
170 algorithm with over 700 storms in multiple storm environments to help understand the
171 variability of the algorithm (Schultz et al. 2011). The choice of the $2*\sigma$ (i.e. $\alpha=2$) in
172 Schultz et al. (2011) is simply a benchmark to which this study is not tied to.

173 3. Analysis and Discussion

174 *3.1 Data and Quality control*

175 As WDSS-II tracks clusters independently of the respective total lightning
176 activity, the number of the identified LJ0 and LJ1 clusters is considerably different. For
177 instance more than 2,000 clusters are classified as LJ0 at $\alpha=2.0 \text{ f m}^{-2}$ and $\text{FRT}=10 \text{ f m}^{-1}$
178 whereas less than 200 are classified as LJ1 for the same α and FRT values. To ensure a
179 comparable sample size and improve the representativeness of the data, we report on the
180 LJ0 and LJ1 clusters that exhibit sustained total lightning activity for more than 95%
181 during their lifespan (e.g., if a cluster is tracked for 100 minutes, the cluster must exhibit
182 total lightning activity greater than zero for at least 95 minutes). This quality constraint
183 (QC1) may classify a slightly different number of clusters depending on the employed
184 lightning detection system. An additional quality constraint (QC2) is applied to the
185 clusters that start or end at a flash rate that is notably higher than zero (set to $>10 \text{ f m}^{-1}$).
186 Typically, these cases represent merging or splitting clusters or clusters that
187 entered/exited the effective radius of the LMA with high flash rates. QC2 also takes
188 care of potential problems with MESH/VIL repetitiveness due to distance from the

189 radar. Given that the study explores aspects such as the storm duration, the clusters that
190 failed to conform to QC2 are omitted from the analysis. Figure 1 illustrates examples
191 from a tracked cluster that exhibits a problematic tracking (e.g. cluster entering the area
192 with already high flash rates, Fig. 1a), a normal tracking (i.e. comply with both QC1 and
193 QC2, Fig. 1b), a LJ0 cluster (Fig. 1c) and a LJ1 cluster (Fig. 1d) of comparable flash
194 rates.

195 All three lightning detection systems indicate that the number of LJ1 clusters
196 decreases as the α and FRT values increase (i.e. fewer clusters at higher α and FRT
197 values, Fig. 2b, d, and f). Unlike the LJ1, the number of tracked LJ0 clusters increases as
198 the values of α and FRT increase (Fig. 2a, c, and e). The latter should be expected since
199 a LJ0 at e.g. $\alpha=2.0$ and $FRT=10 \text{ f m}^{-1}$ will also not exhibit LJ at higher α or FRT values.

200 *3.2 The Autocorrelation function of LJ0 and LJ1 Flash Time Series.*

201 Autocorrelation is an essential tool for describing the independence of sequential
202 values in a time series. A slow (fast) decaying autocorrelation function with time (i.e.
203 lag) indicates a consistent (random) behavior of the variable under consideration
204 (Bowerman and O'Connell 1979). For example, a slow-decaying autocorrelation
205 function of lightning activity time-series would signal a coherent behavior in the storm's
206 updraft speed and volume (e.g., Schultz et. al. 2009; 2011; Schultz et al. 2014).
207 Consequently, autocorrelation can elaborate on whether the presence of a LJ relates to a
208 numerically random increase in the total lightning activity or points to a more persistent
209 feature of the storm's dynamical evolution. The autocorrelation function is computed for

210 the flash rates of LJ0 and LJ1, by introducing a time lag that ranges from 1 to $+N/2$
211 minutes, where N is the number of 1-minute intervals during which the cluster is tracked
212 (i.e., lifespan). The lag at which the Pearson correlation is reduced below the 95%
213 significance level denotes the “*e-folding*” time.. Figure 3 illustrates the average e-folding
214 times for the LJ0 and LJ1 clusters for different α and FRT values. The corresponding
215 results (Fig. 3) show longer e-folding times for the LJ1 clusters. For example, the e-
216 folding times for the LJ1 at $\alpha=2.0$ and $FRT=15 \text{ f m}^{-1}$ are computed as ~ 12 min for LMA,
217 12.7 min for the ENTLN, and 11.5 min for the NLDN. Conversely, the e-folding times
218 for the LJ0 for the same α and FRT values are consistently less than ~ 4.0 min for all
219 three lightning detection systems and any given α and FRT value. Moreover, the fact
220 that the e-folding times for LJ1 clusters increase as both α and FRT values also increase,
221 illustrates a key observation that emphasizes the non-redundant numerical role of both
222 variables α and FRT in the LJ algorithmic implementation (Schultz et al. 2009; 2011).

223 *3.3 Comparison of storm severity potential and physical characteristics between* 224 *the LJ0 and LJ1 clusters.*

225 The previous section studied the LJ0 and LJ1 clusters exclusively from the
226 standpoint of the flash rate temporal variation. This section explores the mean values of
227 storm attributes derived from WDSS-II. As Fig. 4 demonstrates, the LJ1 clusters exhibit
228 a longer lifespan than the respective LJ0, and this observation is consistent throughout
229 the three lightning detection systems and all α and FRT values. For example, for $\alpha=2.0$
230 and $FRT=15 \text{ f m}^{-1}$, the average lifespan is 80 min, whereas the respective LJ0 lifespan is

231 approximately 35 min. Similar behavior is evident for the mean flash rate (normalized
232 by the cluster's footprint area, $f \text{ m}^{-1} \text{ km}^{-2}$, Fig. 5), MESH (Fig. 6) and VIL (Fig. 7)
233 values.

234 In particular, Fig. 5 indicates that on average, the LJ1 clusters exhibit ~ 4 -5 times
235 higher flash rates than the respective LJ0. For instance, the average LJ1 flash rates for α
236 $= 2.0$ and $\text{FRT} = 15 \text{ f m}^{-1}$ are $\sim 0.054 \text{ f m}^{-1} \text{ km}^{-2}$ as opposed to $\sim 0.015 \text{ f m}^{-1} \text{ km}^{-2}$ for the
237 LJ0, an observation that is also consistent across all networks. In turn, the MESH values
238 for the LJ1 clusters range from ~ 11 -18 mm whereas the LJ0 corresponding values range
239 from ~ 6.5 -10 mm (Fig. 6). Likewise, the mean values of VIL are $\sim 18 \text{ kg m}^{-2}$ for the
240 LJ0 and $\sim 25 \text{ kg m}^{-2}$ for the respective LJ1 (Fig. 7). As also highlighted in Section 3.2,
241 higher flash rates, larger MESH and VIL values (Figs. 5-7) are found with increasing α
242 and FRT thresholds. One could argue that it would be expected to have higher
243 magnitudes of weather severity proxies (e.g., MESH, VIL etc.) with higher flash rates.
244 Nevertheless, the previous results also suggest that it is not only the flash rate (i.e., FRT)
245 that exhibits a fundamental physical tie to storm intensity but also its temporal evolution
246 (i.e., α). The above results are also in agreement with the findings by Rudlosky and
247 Fuelberg (2013).

248 *3.4 LJ strength and storm decay time*

249 The results shown in Fig. 4 support that the LJ1 clusters with larger α and FRT
250 relate to storms with longer durations (Fig. 4). Approaching this from a different
251 perspective one can raise the following question: "Does the strength of the final LJ

252 occurrence relate to the remaining lifespan of the cluster?” To address this question the
253 time elapsed from the last LJ occurrence to the last time-step that a cluster is tracked is
254 computed in minutes. Arguably, the results in Fig. 8 corroborate that both α and FRT
255 play a role in the storms’ remaining duration which shows to increase from around 30-
256 35 min for LJ1 of $\alpha = 1.0$ and FRT=10 f m⁻¹ to over 45-60 min for higher α and/or FRT
257 values.

258 **4. Conclusions**

259 The observations herein indicate that the presence of LJ has implications for the
260 storm dynamics, intensity and evolution. The e-folding times are lower for the LJ1
261 clusters. For example the e-folding times for the LJ1 at $\alpha = 2.0$ and FRT=15 f m⁻¹ are
262 computed as ~12 min for LMA, 12.7 min for the ENTLN, and 11.5 min for the NLDN.
263 Conversely, the e-folding times for the LJ0 for the same α and FRT values are
264 consistently less than ~4.0 min for all three lightning detection systems. Through the
265 enhanced updraft hypothesis, these findings indicate that the presence of a LJ signals the
266 storm’s ability to sustain convection.

267 The study also documents that LJ1 clusters last longer and exhibit higher flash
268 rates (area-normalized), MESH and VIL values, further corroborating previous studies
269 that also suggest that the temporal total lightning variability is a dependable proxy for
270 severe weather risk assessment (Williams 2001; Schultz et al. 2009; 2011; Rudlosky and
271 Fuelberg 2013). In addition, the MESH values for the LJ1 clusters range from ~11-18
272 mm whereas the LJ0 respective values range from ~6.5-10 mm (Fig. 5). The mean

273 values of VIL are $\sim 18 \text{ kg m}^{-2}$ for the LJ0 and $\sim 25 \text{ kg m}^{-2}$ for the LJ1 clusters.

274 The results throughout this analysis consistently suggest that there is no
275 redundancy in the role of α and FRT in the LJ numerical implementation. This is shown
276 by the increasing magnitudes of the implicated variables (e.g. e-folding time, MESH,
277 flash rate etc., see Fig.2-7) for LJ1 clusters increase as both α and FRT values also
278 increase. Finally, the study offers further evidence that the presence and temporal
279 coincidence of a LJ could be viewed as a proxy of the storm's expected dissipation.
280 Typically, these values range between 20-60 min depending on the LJ strength with
281 stronger jumps indicating more time until storm decay.

282 Ongoing efforts explore the value of the LJ as a component in the operational
283 severe weather watch/warnings issuance (Schultz et al. 2014). The upcoming Geo-
284 stationary Lightning Mapper (GLM) onboard the GOES-R mission (Goodman et al.
285 2013) will provide continuous monitoring of total lightning activity across the Western
286 Hemisphere. GLM will provide even greater detail on the linkage between temporal
287 lightning variability and the storm evolution over areas where currently related
288 information, including radar, is limited or nonexistent. Importantly, GLM will provide
289 continuous coverage of total lightning over a large domain to evaluate this study on the
290 global scale.

291 **Acknowledgements**

292 We acknowledge the support by GOES-R System Program as part of the GOES-R
293 Proving Ground and Risk Reduction programs. The first and second authors also

294 acknowledge the support by the UAH Individual Investigator Distinguished Research
295 awards for 2014. C. Schultz would like to acknowledge the NASA Pathways Intern
296 Program, which provided the funding for support of this work. Lightning data were
297 kindly provided by 1) Geoffrey Stano at the NASA-Short-term Prediction Research and
298 Transition Center (SPoRT) 2) Earth Networks for the ENTLN data and 3) Vaisala for the
299 NLDN data. We would also like to extend a sincere thanks to the three anonymous
300 reviewers who helped us improve this paper.

301

302 4. **References**

303 Amburn, S., and P. Wolf, 1996: VIL Density as a Hail Indicator. 18th Conference on
304 Severe Local Storms. San Francisco, CA, Amer. Meteor. Soc., 581-585.

305

306

307

308 Bowerman, B. L., and O'Connell, R. T., 1979: *Time Series and Forecasting*, Duxbury
309 Press, North Scituate, Massachusetts.

310

311 Bruning, Eric C., Donald R. MacGorman, 2013: Theory and Observations of
312 Controls on Lightning Flash Size Spectra. *J. Atmos. Sci.*, **70**, 4012–4029.

313 Carey, L. D. and S. A. Rutledge, 2000: On the relationship between precipitation
314 and lightning in tropical island convection: A C-band polarimetric radar study.
315 Monthly Weather Review, 128, 2687–2710.

316 Carey, L. D., W. A. Petersen, and C. J. Schultz, 2009: A statistical framework for
317 the development and evaluation of a lightning jump algorithm. Preprints, Fourth
318 Conference on the Meteorological Applications of Lightning Data, Phoenix, AZ,
319 Amer. Meteor. Soc. d

320 Chronis T., Williams E, Anagnostou E., Walt Petersen, 2007: Lightning as a precursor
321 of tropical cyclogenesis, Eos Trans. AGU, 88(40), 397, 10.1029/2007EO400001.

322

323 Cintineo, L. J., Michael J. Pavolonis, Justin M. Sieglaff, Daniel T. Lindsey, 2014:
324 An Empirical Model for Assessing the Severe Weather Potential of Developing
325 Convection

326

327 Cintineo, L. J., Travis M. Smith, Valliappa Lakshmanan, Harold E. Brooks, Kiel
328 L. Ortega, 2012: An Objective High-Resolution Hail Climatology of the
329 Contiguous United States. Wea. Forecasting, 27, 1235–1248. doi:
330 <http://dx.doi.org/10.1175/WAF-D-11-00151.1>

331

332 Cummins, K. L., E. A. Bardo, W. L. Hiscox, R. B. Pyle, and A. E. Pifer, 1995:
333 NLDN '95: A combined TOA/MDF technology upgrade of the U.S. National
334 Lightning Detection Network, 1995: International Aerospace and Ground
335 Conference on Lightning and Static Electricity, Williamsburg, Virginia, 26-28
336 Sept 1995.

337

338 Cummins, K., E. P. Krider and M. Malone, 1998: The U.S. National Detection
339 network and applications of cloud-to-ground lightning data by electric power
340 utilities, IEEE Trans. on Electromagnetic Compatibility, Vol. 40, no. 4.

341

342

343 Cummins, K. L., J. Cramer, C. Biagi, E. P. Krider, J. Jerauld, M. Uman, and V.
344 Rakov, 2006: The U.S. National Lightning Detection Network: Post-upgrade
345 status. Second Conference on Meteorological Applications of Lightning Data,
346 Atlanta, Georgia, American Meteorological Society.

347

348 Cummins, K. L., and M. J. Murphy, 2009: An overview of lightning locating
349 systems: History, techniques, and data uses, with an in-depth look at the U.S.
350 NLDN. IEEE Trans. on Electromagnetic Compatibility, 51, 3, 499- 518.

351

352 Deierling, W., and W. A. Petersen, 2008: Total lightning activity as an indicator
353 of updraft characteristics, *J. Geophys. Res.*, 113, D16210,
354 doi:[10.1029/2007JD009598](https://doi.org/10.1029/2007JD009598).

355

356 Emersic, C. and C.P.R. Saunders, 2010: Further laboratory investigations into the
357 relative diffusional growth rate theory of thunderstorm electrification. *Atmos.*
358 *Res.*, 98, doi:[10.1016/j.atmosres.2010.07.011](https://doi.org/10.1016/j.atmosres.2010.07.011)

359

360 Gatlin, P., Goodman, S.J., 2010: A total lightning trending algorithm to identify
361 severe thunderstorms. *J. Atmos. Ocean. Technol.* 27, 3–22.

362

363 Goodman, S. J., D. E. Buechler, P. D. Wright, and W. D. Rust, 1988: Lightning
364 and precipitation history of a microburst-producing storm. *Geophys. Res. Lett.*,
365 15, 1185–1188.

366 Goodman, S. J., R. Blakeslee, H. Christian, W. Koshak, J. Bailey, J. Hall, E.
367 McCaul, D. Beuchler, C. Darden, J. Burks, T. Bradshaw, P. Gatlin, 2005: The
368 North Alabama Lightning Mapping Array: Recent severe storm observations and
369 future prospects. *Atmos. Res.*, **76**, 423-437.

370

371 Goodman S, Blakeslee R, Koshak W, Mach D, Bailey J, Buechler D, Carey L, Schultz
372 C, Bateman M, Jr. E, et al. *The GOES-R Geostationary Lightning Mapper (GLM)*.
373 Atmospheric Research. 2013;125-126 34-49.

374

375 Greene, D. R., and R. A. Clark, 1972: Vertically integrated liquid water- A new
376 analysis tool. *Mon. Wea. Rev.*, 100, 548-552

377

378

379

380 Koshak, W. J., R. J. Solakiewicz, R. J. Blakeslee, S. J. Goodman, , H. J. Christian,
381 J. M. Hall, J. C. Bailey, E. P. Krider, M. G. Bateman, D. J. Boccippio, D. M.
382 Mach, E. W. McCaul, M. F. Stewart, D. E. Buechler, W. A. Petersen, D. J. Cecil,
383 2004: North Alabama Lightning Mapping Array (LMA): VHF source retrieval
384 algorithm and error analyses, *J. Atmos. Oceanic Technol.*, 21, 543-558.

385

386 Keene, K. M., P. T. Schlatter, J. E. Hales, and H. Brooks, 2008: Evaluation of
387 NWS watch and warning performance related to tornadic events. Preprints, 24th
388 Conf. on Severe Local Storms, Savannah, GA, Amer. Meteor. Soc., P3.19.

389 Krehbiel, P. R., 2008: The DC Lightning Mapping Ar- ray. Preprints, Third
390 Conference on Meteorological Ap- plications of Lightning Data, New Orleans,
391 LA, USA, American Meteorological Society. 3.2.

392 Krehbiel, P. R., 2008: The DC Lightning Mapping Array. Preprints, Third Conf.
393 on Meteorological Applications of Lightning Data, New Orleans, LA, Amer.
394 Meteor. Soc., 3.2. [Available online at
395 <http://ams.confex.com/ams/pdfpapers/129095.pdf>.]

396 Lakshmanan, V., and T. Smith, 2009: Data mining storm attributes from spatial
397 grids. *J. Atmos. Oceanic Technol.*, 26, 2353–2365.

398

399 Lakshmanan, V., K.Hondl, and R.Rabin, 2009: An efficient, general-purpose
400 technique for identifying storm cells in geospatial images,' *J. Ocean. Atmos.*
401 *Tech.*, vol.26, no.3, pp.523-37.

402

403 Lakshmanan, V., T. Smith, G. J. Stumpf, and, K. Hondl, 2007: The Warning
404 Decision Support System–Integrated Information. *Wea. Forecasting*, 22, 596–612.

405 Lang, T. J., and Rutledge, S. A., 2002: Relationships between convective
406 storm kinematics, precipitation, and lightning. *Mon. Wea. Rev.*, 130: 2492–2506.

407

408 Liu C., and Heckman S., 2011: Using Total Lightning Data and Cell Tracking in
409 Severe Weather Prediction, 91st AMS meeting.

410 MacGorman, D. and C. D. Morgenstern, 1998: Some characteristics of cloud to ground
411 lightning in mesoscale convective systems, *J. Geophys. Res.*, 103, D12, 14,011-14,023.

412

413 MacGorman, D.R., Rust, W.D., Schuur, T.J., Biggerstaff, M.I., Straka, J.M., Ziegler,
414 C.L., Mansell, E.R., Bruning, E.C., Kuhlman, K.M., Lund, N.R., Biermann, N.S., Payne,
415 C., Carey, L.D., Krehbiel, P.R., Rison, W., Eack, K.B., Beasley, W.H., 2008. TELEX:
416 The Thunderstorm Electrification and Lightning Experiment. *Bull. Am. Meteorol. Soc.*
417 89, 997–1013.

418

419 McCaul, E. W., J. Bailey, J. Hall, S. J. Goodman, R. Blakeslee, and D. E. Buechler,
420 2005: A flash clustering algorithm for North Alabama Lightning Mapping Array data.
421 Preprints, *Conf. on Meteorological Applications of Lightning Data*, San Diego, CA,
422 Amer. Meteor. Soc., 5.2. [Available online at [http://ams.confex.com/ams/
423 Annual2005/techprogram/paper_84373.htm](http://ams.confex.com/ams/Annual2005/techprogram/paper_84373.htm)].

424 Murphy, M. J. and A. Nag, 2014: Enhanced cloud lightning performance of the U.S.
425 National Lightning Detection Network following the 2013 upgrade, 23rd International
426 Lightning Detection Conference & 5th International Lightning Meteorology Conference,
427 18-21 March, Tucson, Arizona.

428

429 Petersen, W. A., H. J. Christian, and S. A. Rutledge, 2005: TRMM observations
430 of the global relationship between ice water content and lightning. *Geophys. Res.*
431 *Let.*, 32, doi: 10.1029/2005GL023236.

432 Scott D. Rudlosky, S D., and Henry E. Fuelberg, 2010: Pre- and Postupgrade Distributions of NLDN
433 Reported Cloud-to-Ground Lightning Characteristics in the Contiguous United States. *Mon. Wea. Rev.*,
434 **138**, 3623ea. Re doi: <http://dx.doi.org/10.1175/2010MWR3283.1>
435

436 Rudlosky, Scott D., and Henry E. Fuelberg. 2013: Documenting Storm Severity in
437 the Mid-Atlantic Region Using Lightning and Radar Information, *Monthly*
438 *Weather Review* 141, no. 9: 3186-3202.

439

440 Saunders, C. P. R., 1993: A Review of Thunderstorm Electrification Processes. *J.*
441 *Appl. Meteor.*, 32, 642–655.

442 Saunders, C. P. R., H. Bax-Norman, C. Emersic, E. E. Avila, and N. E.
443 Castellano, 2006: Laboratory studies of the effect of cloud conditions on
444 graupel/crystal charge transfer in thunderstorm electrification. *Quart. J. Roy.*
445 *Meteor. Soc.*, 132, 2653-2673.

446 Schultz, C. J. L.D. Carey, E. V. Schultz, R. J. Blakeslee and S. J. Goodman,
447 2014: Physical and dynamical linkages between lightning jumps and storm
448 conceptual models. Conference Proceedings 15th International Conf. on
449 Atmospheric Electricity. Norman, OK.

450 Schultz, C. J., W. A. Petersen, L. D. Carey, 2011: Lightning and Severe
451 Weather: A Comparison between Total and Cloud-to-Ground Lightning Trends.
452 Wea. Forecasting, 26, 744–755.

453 Schultz, C. J., W. A. Petersen, and L. D. Carey, 2009: Preliminary
454 development and evaluation of lightning jump algorithms for the real-time
455 detection of severe weather. J. Appl. Meteor. Climatol., 48, 2543–2563.

456 Shafer, Mark A., Donald R. MacGorman, Frederick H. Carr, 2000: Cloud-to-
457 Ground Lightning throughout the Lifetime of a Severe Storm System in
458 Oklahoma. Mon. Wea. Rev., 128, 1798–1816.

459 Stumpf, G.J., T. M. Smith and J. Hocker, 2004: New hail diagnostic
460 parameters derived by integrating multiple radars and multiple sensors. Preprints,
461 22nd Conf. on Severe Local Storms, Hyannis, MA, Amer. Meteor. Soc., CD-
462 ROM, P7.8.

463 Uman, 1987: The Lightning Discharge, Academic Press, pp. 183

464 Takahashi, T., 1978: Riming electrification as a charge generating mechanism

465 Thomas, R. J., P. R. Krehbiel, W. Rison, S. J. Hunyady, W. P. Winn, T. Hamlin,
466 and J. Harlin, 2004: Accuracy of the lightning mapping array. J. Geophys. Res.,
467 109, D14207, doi:10.1029/2004JD004549.

468 Thomas, R., P. Krehbiel, W. Rison, J. Harlin, T. Hamlin, and N. Campbell, 2003:
469 The LMA flash algorithm. Proc. 12th Int. Conf. on Atmospheric Electricity,
470 Versailles, France, International Commission on Atmospheric Electricity, 655–
471 656.

472 Trapp, R. J., D. M. Wheatly, N. T. Atkins, and R. W. Przybylinski, 2006:
473 Buyer beware: Some words of caution on the use of severe wind reports in
474 postevent assessment and research. *Wea. Forecasting*, 21, 408–415.

475 Vonnegut, B., 1963: Some facts and speculation concerning the origin and
476 role of thunderstorm electricity. *Severe Local Storms, Meteor. Monogr., Amer.*
477 *Meteor. Soc.*, 224–241.

478 water on thunderstorm charging, *J. Geophys. Res.*, 96, 11,007–11,017,
479 doi:10.1029/91JD00970.

480 *Wea. Forecasting*. In Press. [http://journals.ametsoc.org/doi/pdf/10.1175/WAF-D-](http://journals.ametsoc.org/doi/pdf/10.1175/WAF-D-13-00113.1)
481 13-00113.1

482 Williams, E. R., 1985: Large scale charge separation in thunderclouds. *J.*
483 *Geophys. Res.*, 90, 6013–6025.

484 Williams, E. R., Bob Boldi, Anne Matlin, Mark Weber, Steve Hodanish,
485 Dave Sharp, Steve Goodman, Ravi Raghavan, Dennis Buechler, 1999: The

486 behavior of total lightning activity in severe Florida thunderstorms, Atmospheric
487 Research, Volume 51, Issues 3–4, Pages 245-265.

488 Williams, E.R., 2001: The Electrification of Severe Storms, Chapter 13 in Severe
489 Convective Storms, Ed., C.A. Doswell, III, Meteorological Monograph, Vol. 28,
490 No. 50, 527-561.

491 Witt, A., M. D. Eilts, G. J. Stumpf, J. T. Johnson, E. D. Mitchell, and K. W.
492 Thomas, 1998: An enhanced hail detection algorithm for the WSR-88D. Wea.
493 Forecasting, 13, 286-303.

494

495 **Figure Captions**

496 Figure 1: Tracked cluster that exhibits a problematic tracking (e.g. cluster entering the area with already high flash rates,
497 Fig.1a), a normal tracking (i.e. comply with both QC1 and QC2, Fig.1b), a LJ0 cluster (Fig.1c) and a LJ1 cluster (Fig.1d) of
498 comparable flash rates.

499

500 Figure 2: The identified number of LJ0/LJ1 clusters as a function of FRT (x-axis, $f m^{-1}$) and α (y-axis), LMA-
501 a/b, ENTLN-c/d and NLDN-e/f

502 Figure 3: Mean e-folding time (min) for LJ0/LJ1, as a function of FRT (x-axis, $f m^{-1}$) and α (y-axis), LMA-
503 a/b, ENTLN-c/d and NLDN-e/f

504

505 Figure 4: Mean life-span (min) for LJ0/LJ1, as a function of FRT (x-axis, $f m^{-1}$) and α (y-axis), LMA-a/b,
506 ENTLN-c/d and NLDN-e/f

507 Figure 5: Mean area-normalized flash rate ($f \text{ m}^{-1} \text{ km}^{-2}$) for LJ0/LJ1, as a function of FRT (x-axis, $f \text{ m}^{-1}$) and α
508 (y-axis,), LMA-a/b, ENTLN-c/d and NLDN-e/f

509 Figure 6: Mean MESH (mm) for LJ0/LJ1, as a function of FRT (x-axis, $f \text{ m}^{-1}$) and α (y-axis,), LMA-a/b,
510 ENTLN-c/d and NLDN-e/f

511 Figure 7: Mean VIL (kg m^{-2}), for LJ0/LJ1 as a function of FRT (x-axis, $f \text{ m}^{-1}$) and α (y-axis,), LMA-a/b,
512 ENTLN-c/d and NLDN-e/f

513 Figure 8: Time elapsed until the storm dissipation for LJ1 (min) (LMA-a, ENTLN-b and NLDN-c) as a
514 function of FRT (x-axis, $f \text{ m}^{-1}$) and α (y-axis,).

515

516

517

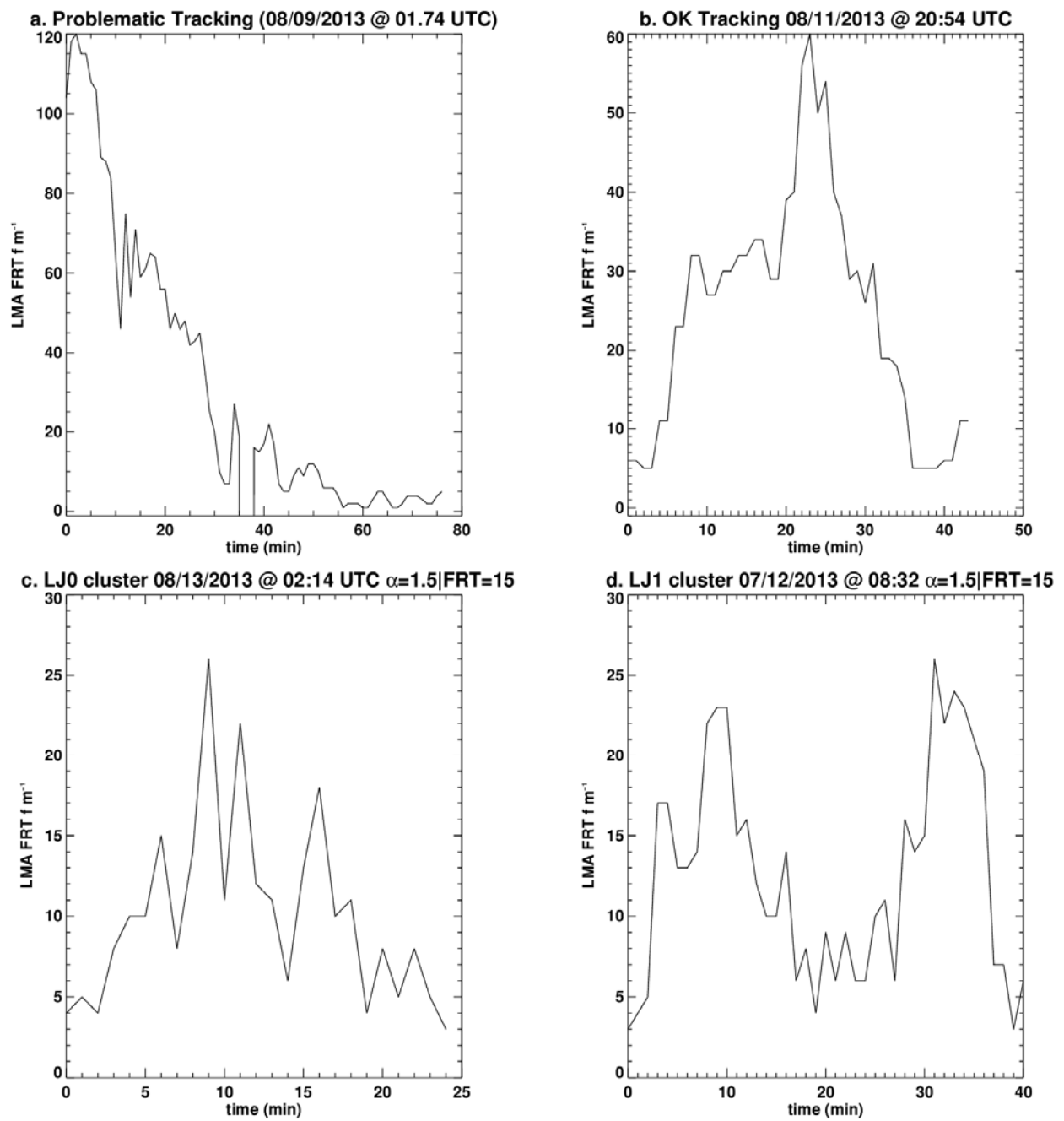
518

519

520

521

522



523

524

525 Figure 1: Tracked cluster that exhibits a problematic tracking (e.g. cluster entering the area with already high flash rates,
 526 Fig.1a), a normal tracking (i.e. comply with both QC1 and QC2, Fig.1b), a LJ0 cluster (Fig.1c) and a LJ1 cluster (Fig.1d) of
 527 comparable flash rates.

528

529

530

531

532

533

534

535

536

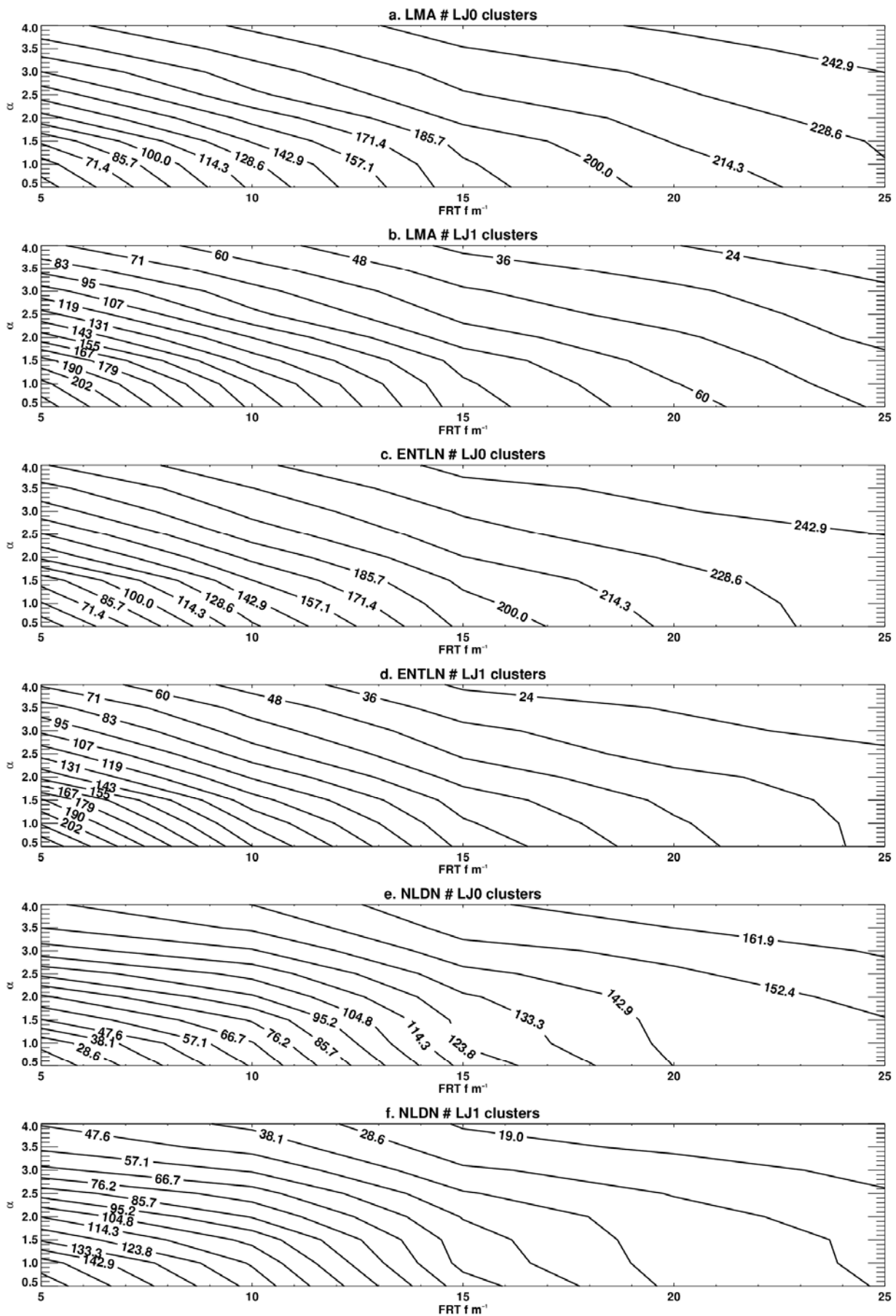
537

538

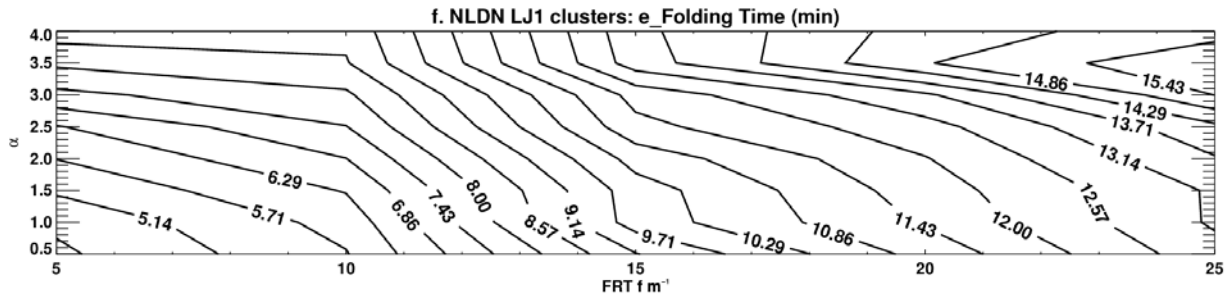
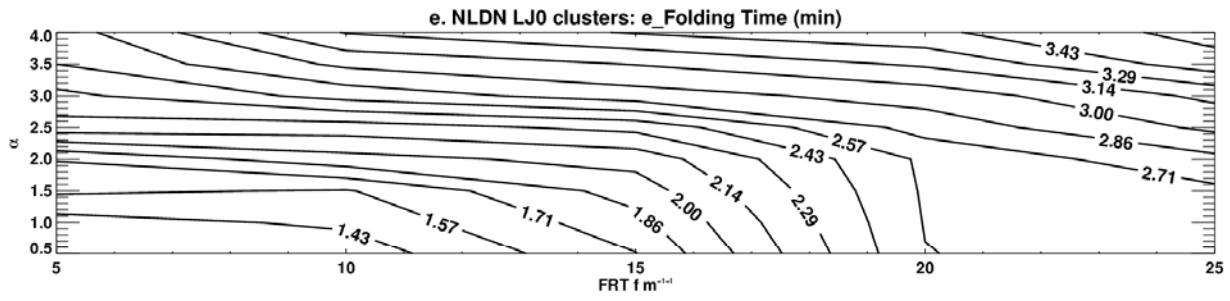
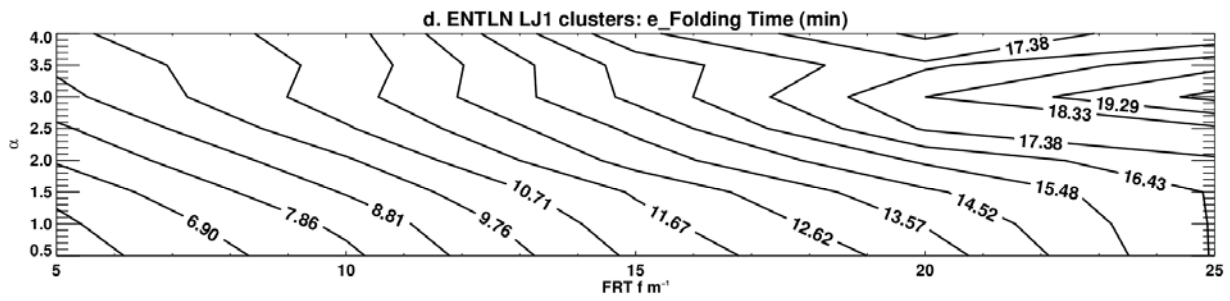
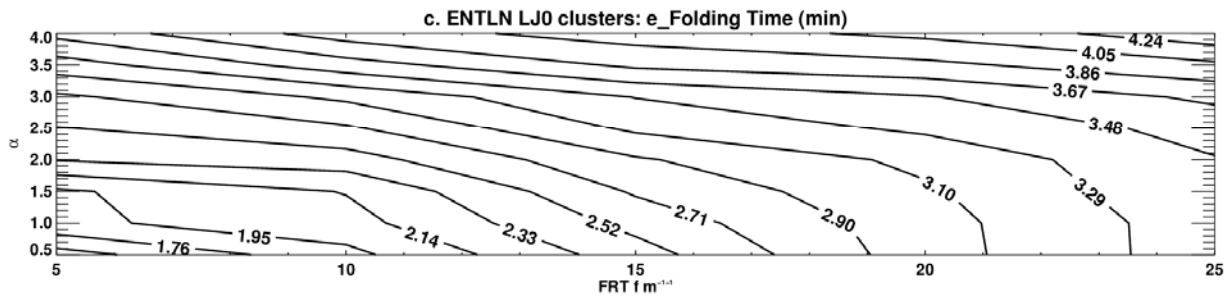
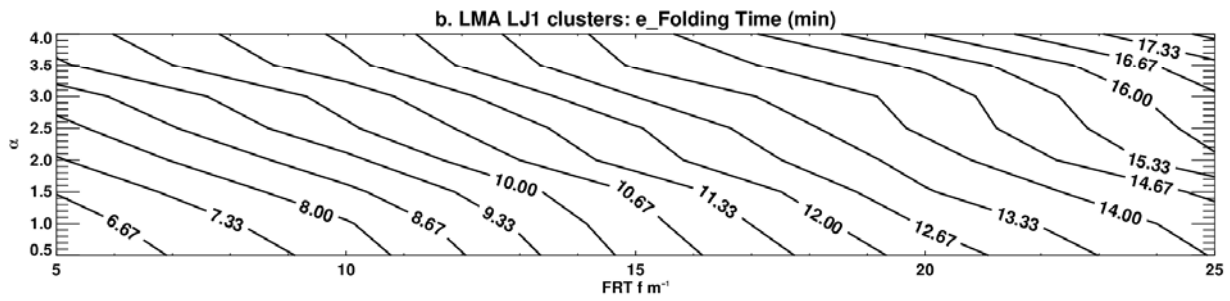
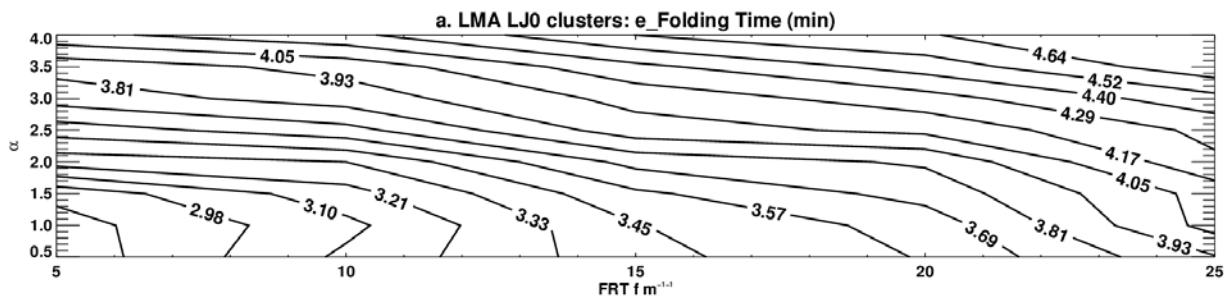
539

540

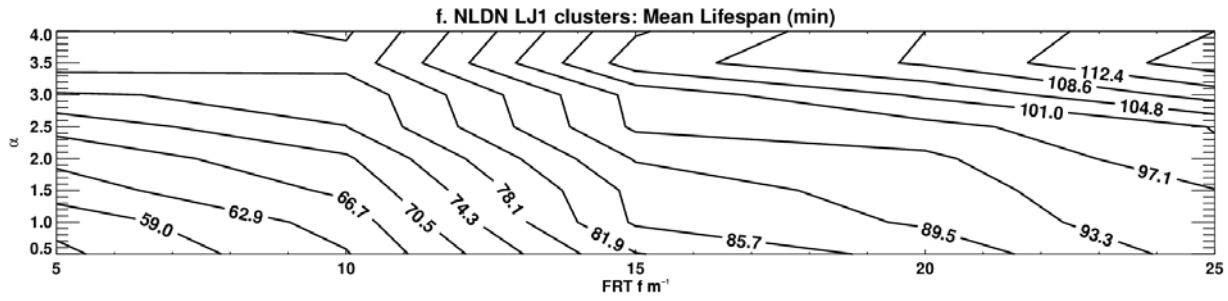
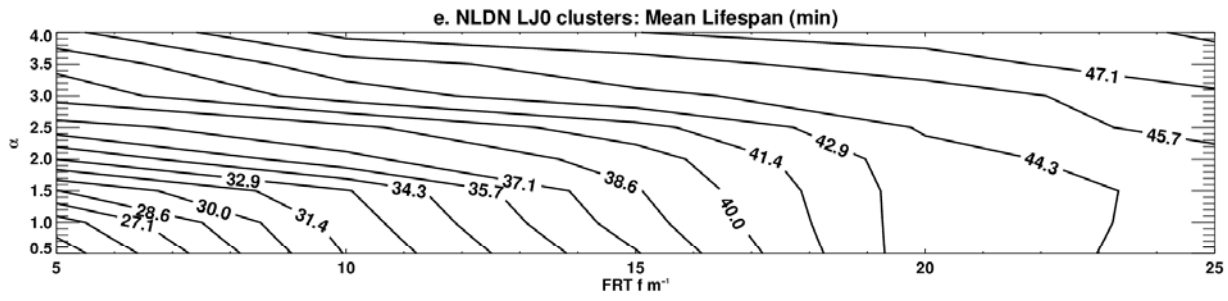
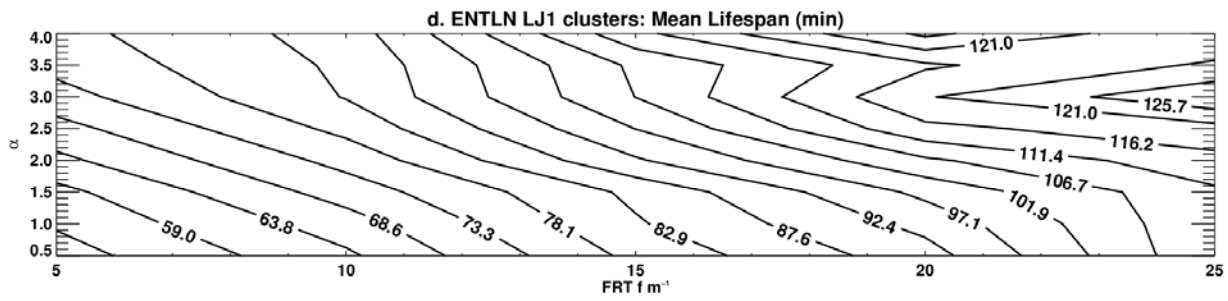
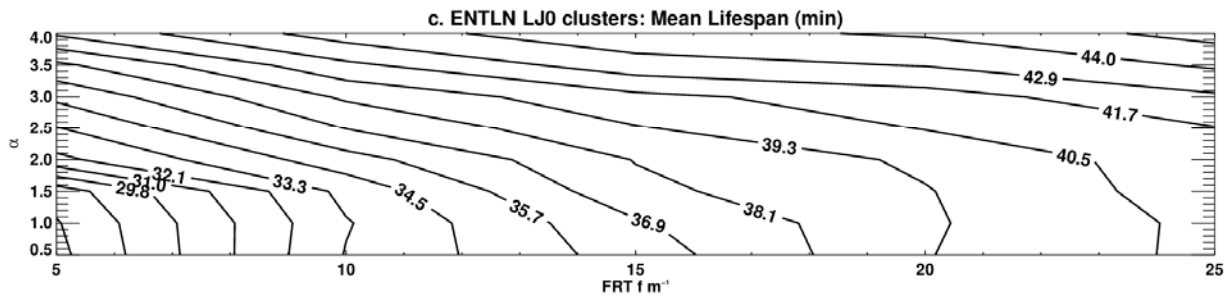
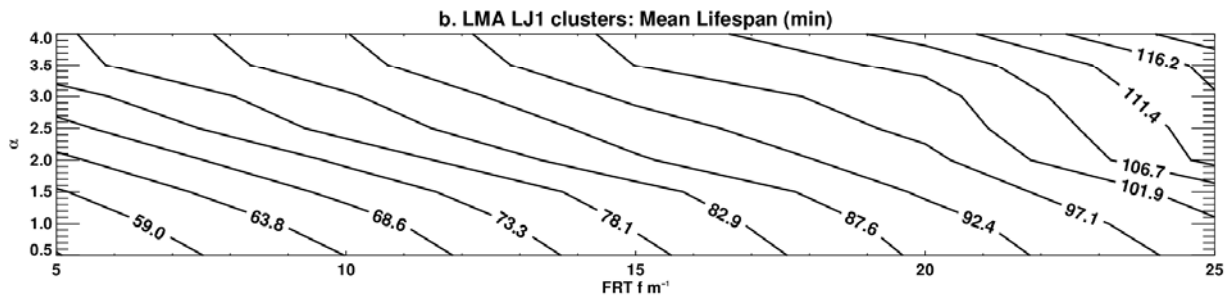
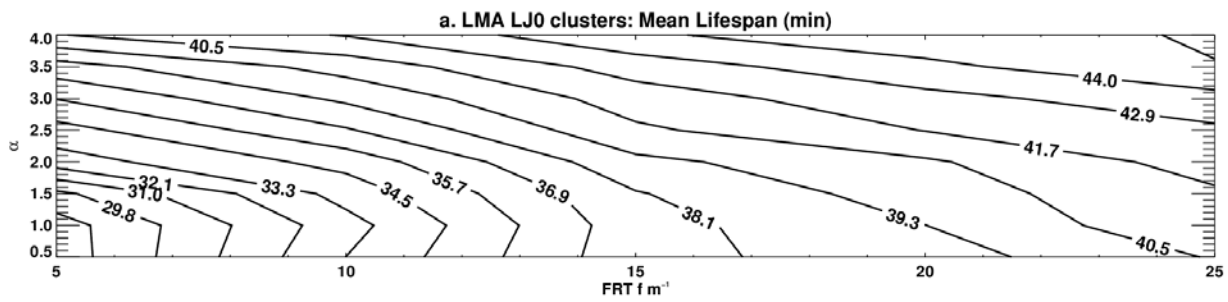
541



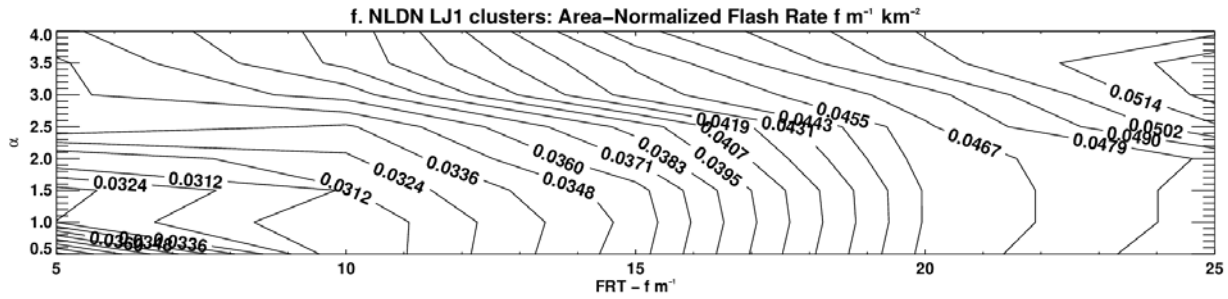
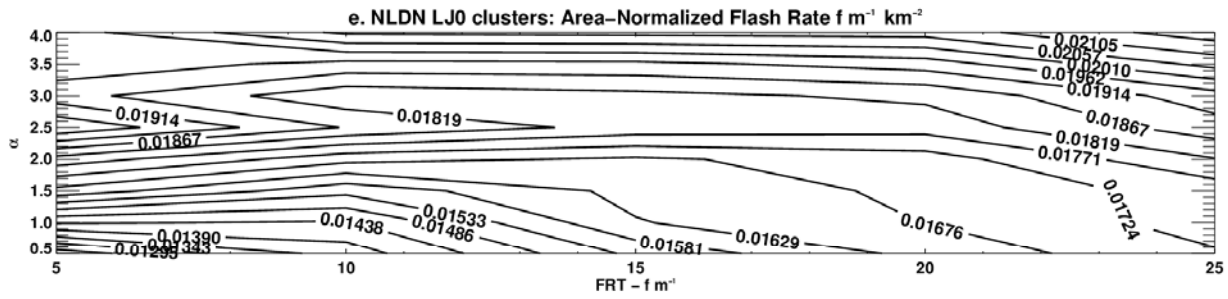
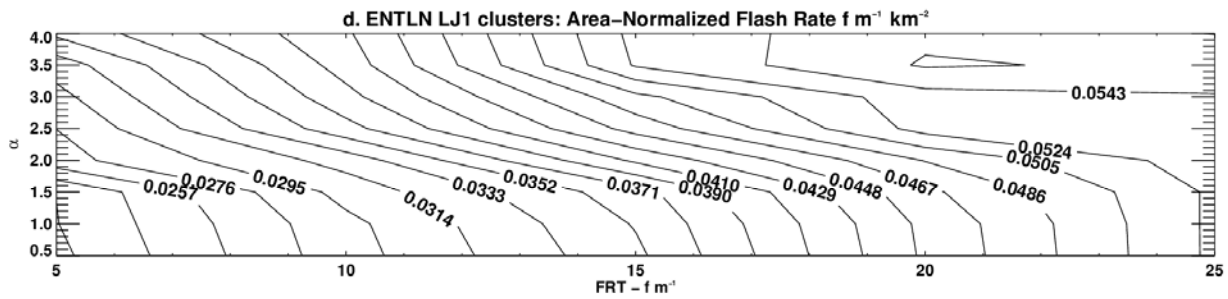
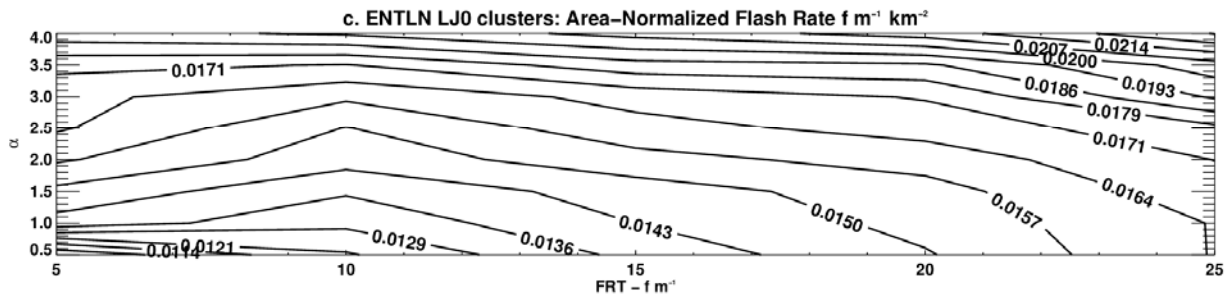
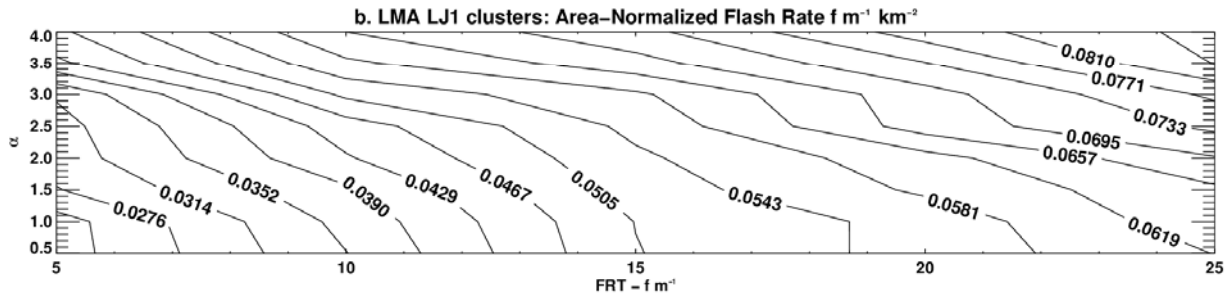
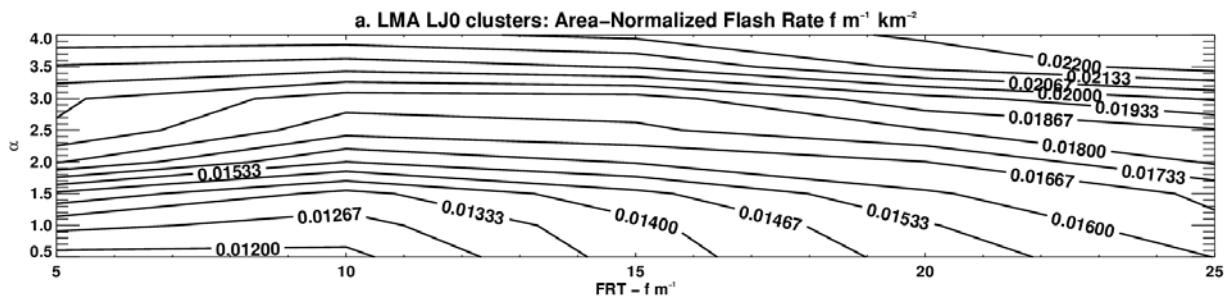
543 Figure 2: The identified number of LJ0/LJ1 clusters as a function of FRT (x-axis, $f m^{-1}$) and α (y-axis), LMA-
544 a/b, ENTLN-c/d and NLDN-e/f
545
546
547
548
549
550
551
552
553
554
555
556
557
558
559
560
561
562



564 Figure 3: Mean e-folding time (min) for LJ0/LJ1, as a function of FRT (x-axis, $f\text{ m}^{-1}$) and α (y-axis), LMA-
565 a/b, ENTLN-c/d and NLDN-e/f
566
567
568
569
570
571
572
573
574
575
576
577
578
579
580
581
582
583



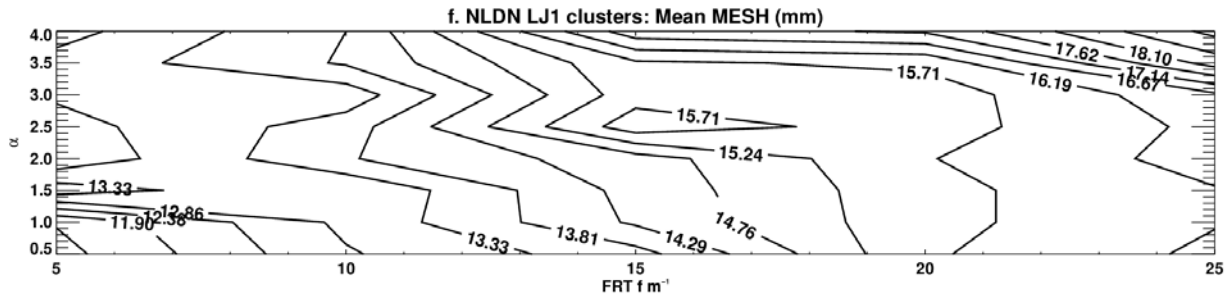
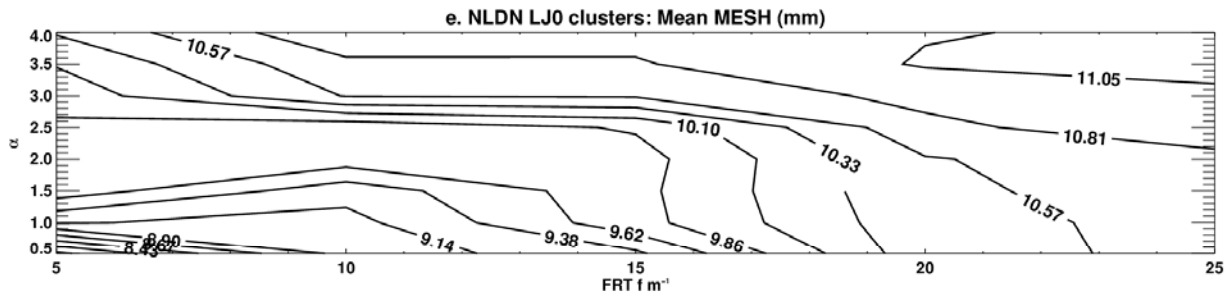
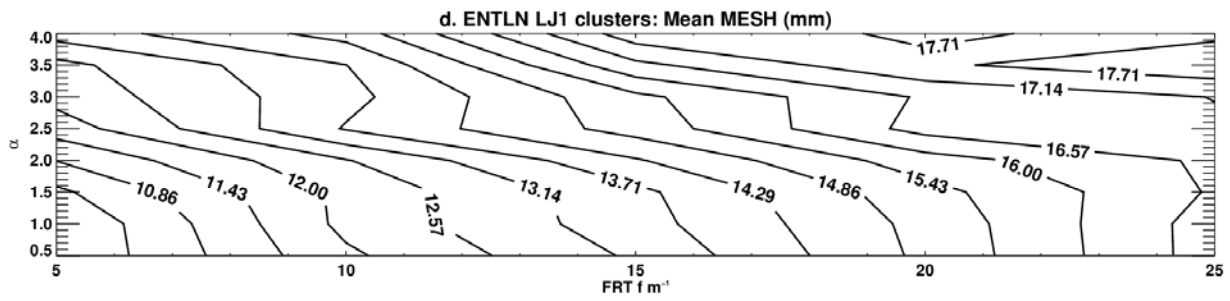
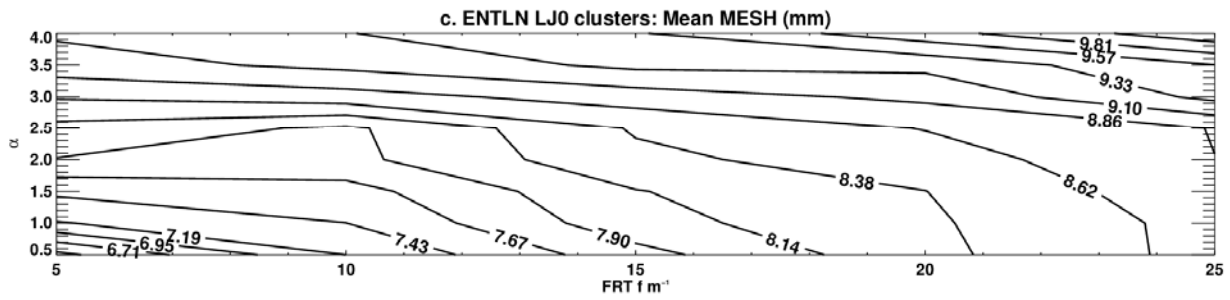
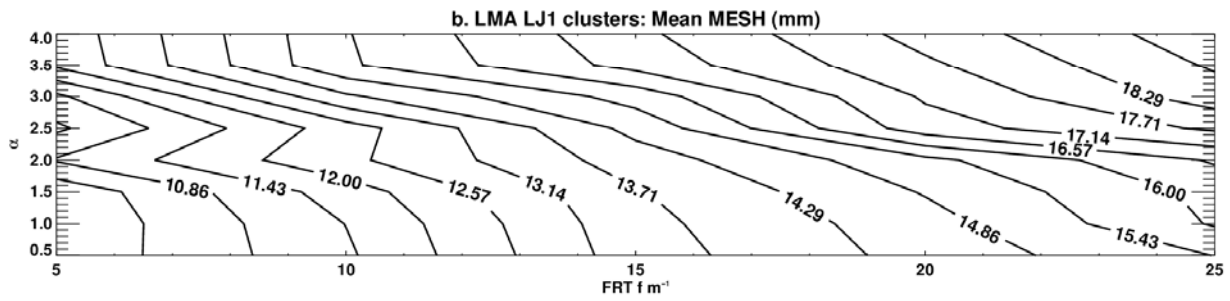
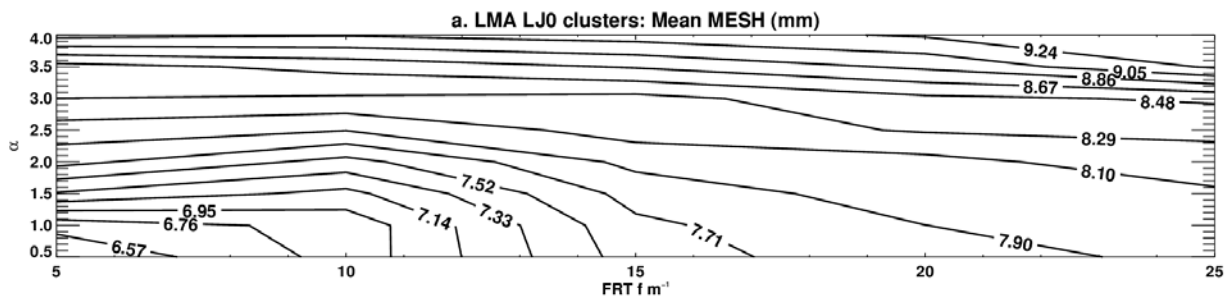
586 Figure 4: Mean life-span (min) for LJ0/LJ1, as a function of FRT (x-axis, $f\ m^{-1}$) and α (y-axis, LMA-a/b,
587 ENTLN-c/d and NLDN-e/f
588
589
590
591
592
593
594
595
596
597
598
599
600
601
602
603
604
605



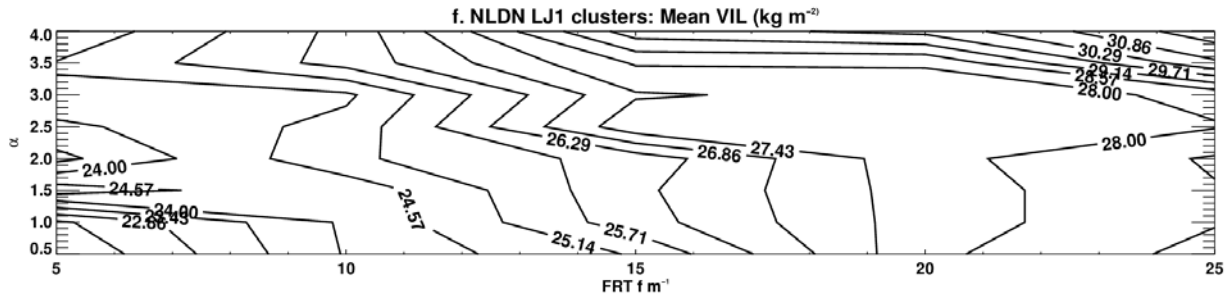
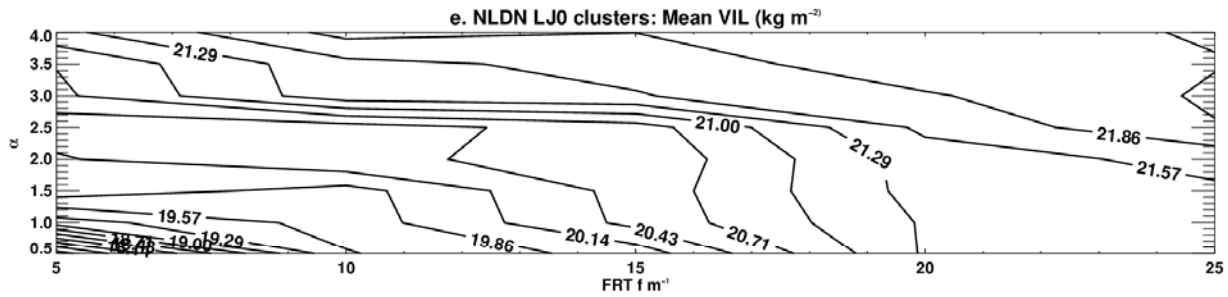
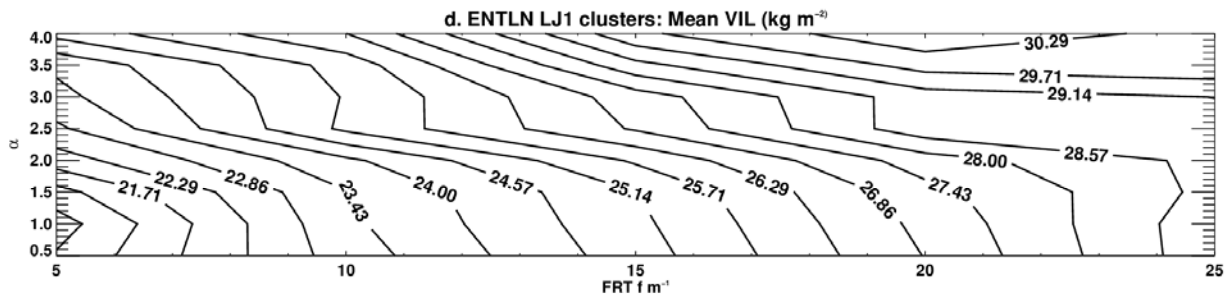
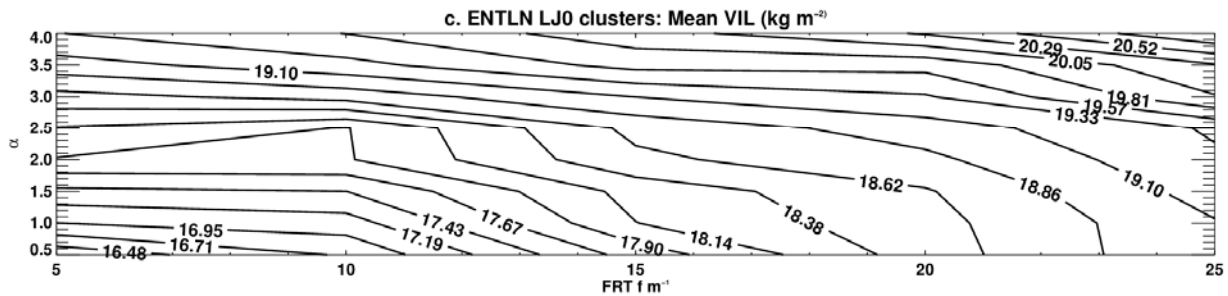
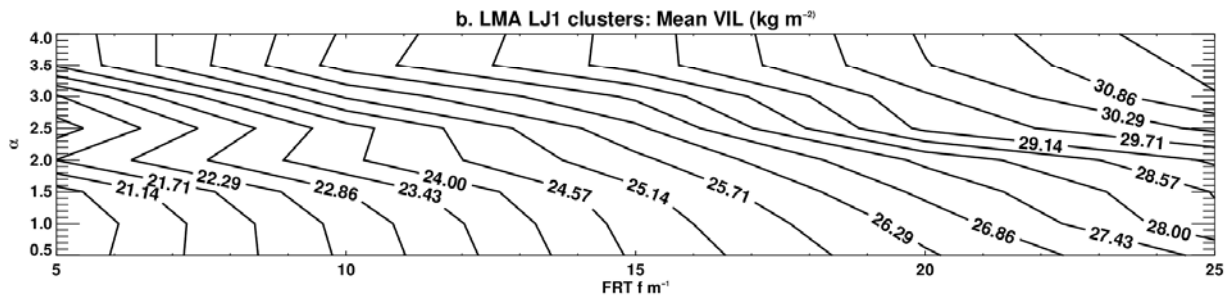
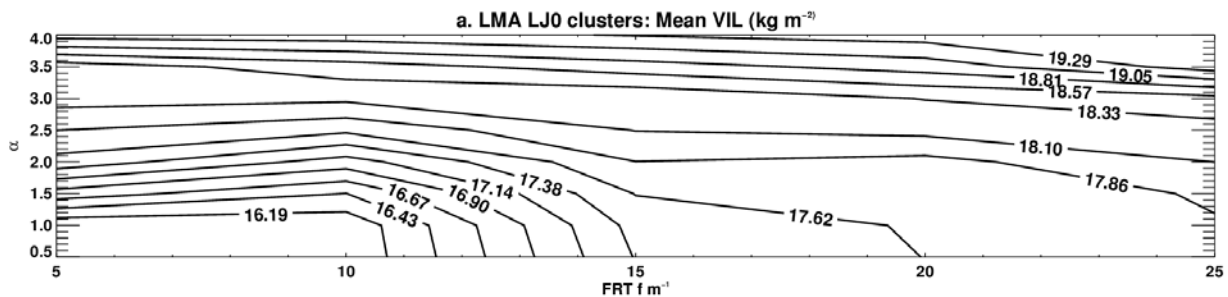
607 Figure 5: Mean area-normalized flash rate ($f \text{ m}^{-1} \text{ km}^{-2}$) for LJ0/LJ1, as a function of FRT (x-axis, $f \text{ m}^{-1}$) and α
608 (y-axis,), LMA-a/b, ENTLN-c/d and NLDN-e/f
609
610
611
612
613
614
615
616
617
618
619
620
621
622
623
624
625
626

627

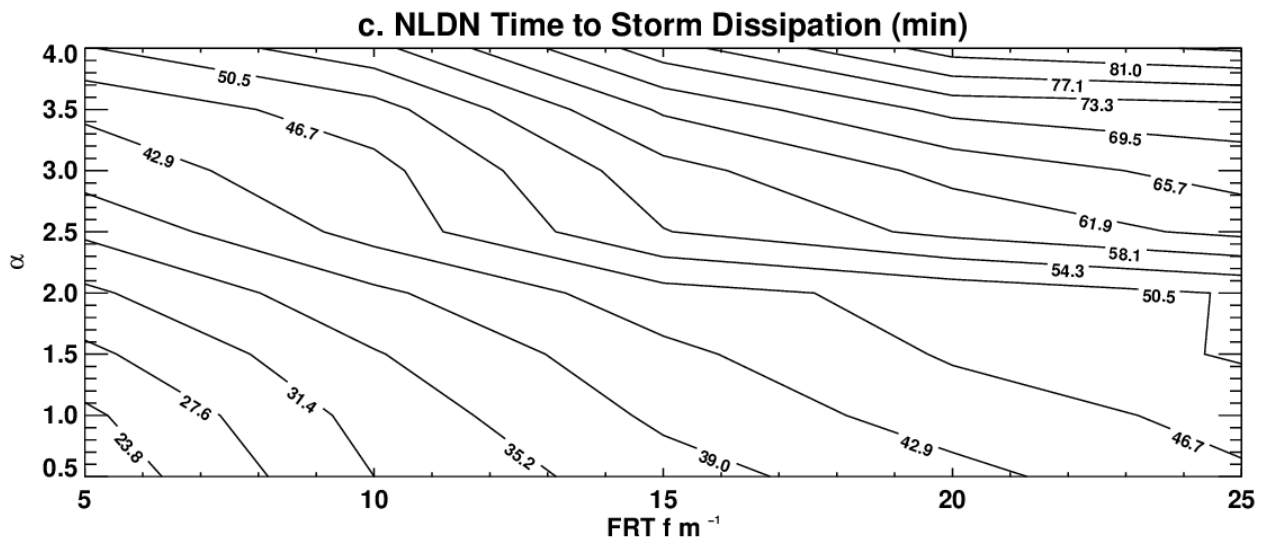
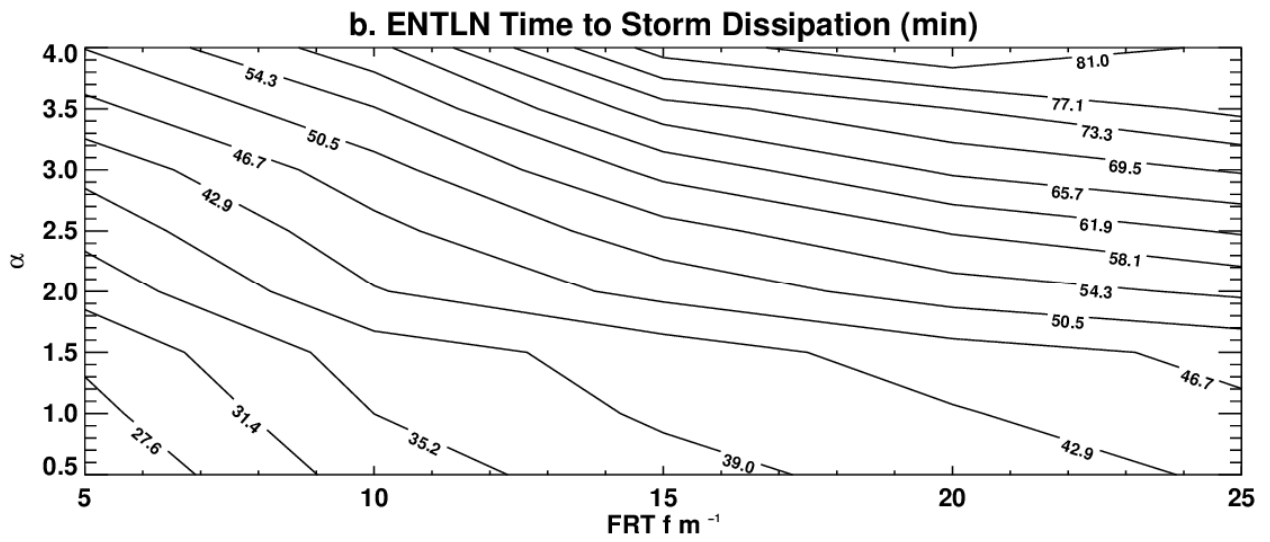
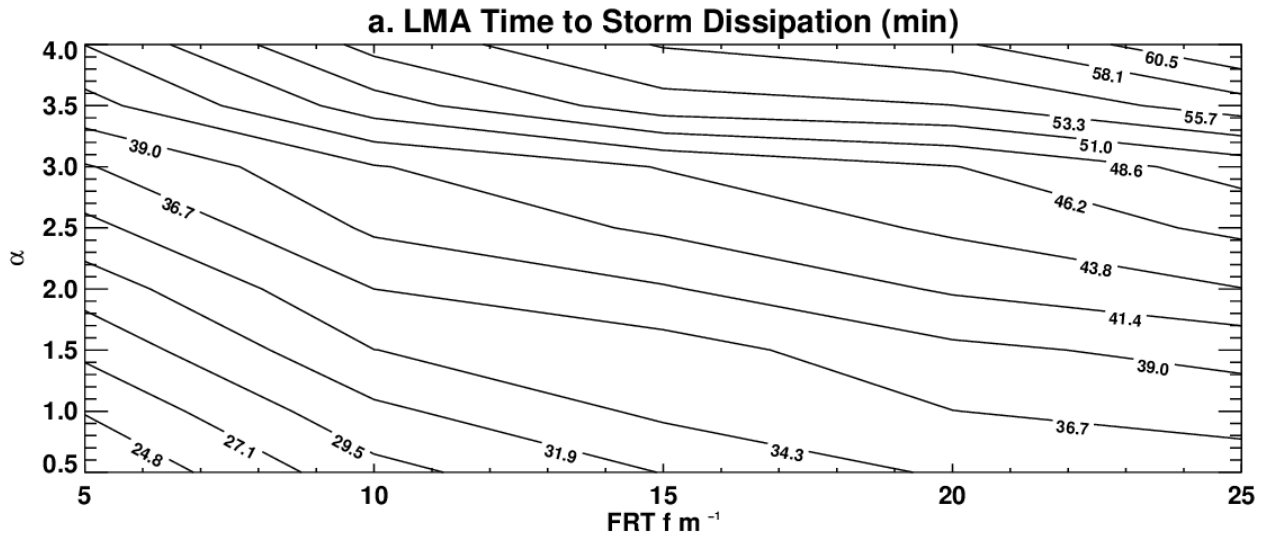
628



630 Figure 6: Mean MESH (mm) for LJ0/LJ1, as a function of FRT (x-axis, $f\ m^{-1}$) and α (y-axis.), LMA-a/b,
631 ENTLN-c/d and NLDN-e/f
632
633
634
635
636
637
638
639
640
641
642
643
644
645
646
647
648
649



651 Figure 7: Mean VIL (kg m^{-2}), for LJ0/LJ1 as a function of FRT (x-axis, f m^{-1}) and α (y-axis), LMA-a/b,
652 ENTLN-c/d and NLDN-e/f
653
654
655
656
657
658
659
660
661
662
663
664
665
666
667
668
669
670



673 Figure 8: Time elapsed until the storm dissipation for LJ1 (min) (LMA-a, ENTLN-b and NLDN-c) as a
674 function of FRT (x-axis, $f m^{-1}$) and \mathcal{Q} (y-axis,).

675

676

677

678

679

680

681

682

683

684

685

686

687

688

689

690

691

692

